Reconfigurable Intelligence Surface with Potential Tunable Meta-devices for 6G: Design and System-level Evaluation

Dongsoo Jun, *Student Member, IEEE,* Wooho Ham, *Student Member, IEEE,* Jang-Yeon Kwon, *Member, IEEE,* Wonbin Hong, *Fellow, IEEE,* Chan-Byoung Chae, *Fellow, IEEE,* and Robert W. Heath, Jr, *Fellow, IEEE*

***Abstract*—Reconfigurable intelligent surface (RIS) technology has emerged as a promising solution to address high-frequency band issues, including low penetration power and increasing shadowing regions, by artificially reconfiguring radio propagation. Previous research on RIS has predominantly relied on metasurfaces based on specific diode-driven devices, and the practical challenges associated with this design have yet to be resolved. This article proposes potential RIS designs through meta-devices, including liquid crystal, 2D material, active metamaterial, and uniquely investigates an electrowetting-based beam tuning methodology. Taking into account the imperfect tuning capabilities of each device, we examine and reflect the relationship between the phase tuning range of RIS and the additional angular variation of the reflected wave. In addition, this article evaluates the RIS performance on a large scale via system-level simulation using 3D ray tracing, reflecting a realistic urban environment. We propose an evaluation methodology that integrates ray tracing with RIS's reflection characteristics and describes RIS-based beamforming throughput performance across various scenarios. Through the empirical evaluation of RIS incorporating meta-device characteristics, this work offers practical intuitions for RIS design contributing to its feasibility and efficiency for B5G/6G standardization and commercialization.**

I. Introduction

FOR the full-fledged realization of the hyper-connected life, high-frequency band systems have been inevitably accompanied in both beyond-5G (B5G) and 6G mobile communications. In order to support the requirements of high-frequency band signals, reconfigurable intelligent surface (RIS) technology has garnered academic attention. RIS can generate a beam with desired properties by dynamically manipulating both device and wave attributes, effectively reconstructing the radio propagation environment. Furthermore, in addition to the signal processing benefits, RIS also holds the potential to improve energy and cost efficiency compared to conventional relay techniques [1]. Due to these efficiencies, interest from industry and standardization bodies has also expanded, and RIS has been mentioned as a candidate topic in the development of the 3GPP Release 19 standards. [2].

D. Jun, W. Ham, J.-Y. Kwon, and C.-B. Chae (corresponding author) are with the School of Integrated Technology, Yonsei University, Seoul, 03722, South Korea (e-mail: {dongsoo.jun, wooho, jangyeon, cbchae}@yonsei.ac.kr).

W. Hong is with the Department of Electrical Engineering, Pohang University of Science and Technology, Pohang, 37673, South Korea (e-mail: whong@postech.ac.kr).

R. W. Heath, Jr is with the Department of Electrical and Computer Engineering, University of California at San Diego, La Jolla, CA 92093, USA (e-mail: rwheathjr@ucsd.edu).

From this perspective, numerous studies have endeavored to optimize the phase tuning matrix of RIS to maximize signal-to-noise-ratio (SNR) or minimize transmit power [3]. However, in reality, no device is capable of achieving 100% phase tuning, necessitating channel modeling that takes into account tuning limitations and accurate reflection angle calculation. In this article, we formulate the relationship between the phase tuning range of the RIS element and the additional reflection angle through geometric modeling in the beam domain. Subsequently, we calculate the control range of the reflected beam direction and apply it to performance evaluation.

Extending from that, when examining RIS designs for phase tuning, variable diode-driven devices are primarily used as unit cell for ease of electromagnetic control and analysis [1]. Yet, alternative devices, with phase and property control capabilities of incident waves, are under investigation in other fields such as optics, some even possessing applicability within the communication band. This article outlines the limitations of the extant diode-based RIS system and proposes potential alternative tunable devices that can be applied to the RIS unit cell, termed meta-devices. In addition, we propose an electrowetting-based RIS beam tuning structure, scarcely reported in existing literature previously, and validate it through implementation at the cell level.

While device technologies for next-generation metasurfaces have been extensively researched and reviewed as discussed in [4], quantitatively relating the tuning physics of various devices to their impact on communication performance presents an additional challenging task. To credibly demonstrate the communication performance of candidate technologies such as new RIS designs, it is necessary to undertake a proof-of-concept (PoC) process that includes testbed implementations, real field trials, and realistic system-level simulation (SLS). However, relative to the aforementioned two approaches [5], [6], there is a scarcity of research that conducts RIS-embedded SLS on a large scale, reflecting realistic environments and propagation topologies. This is due to the difficulty in incorporating the anomalous reflection phenomena of RIS into existing simulators [1]. An alternative method of reflecting the spatial normal vector of the reflector based on the coordinates of the transceivers and RIS into channel modeling was presented in indoor SLS environments [7]. The authors of [8] are in the process of conducting performance assessment using a newly developed simulator named Coffee Grinder that includes the reflection functions of RIS, though an open-access version is not yet available. Although these approaches are gradually

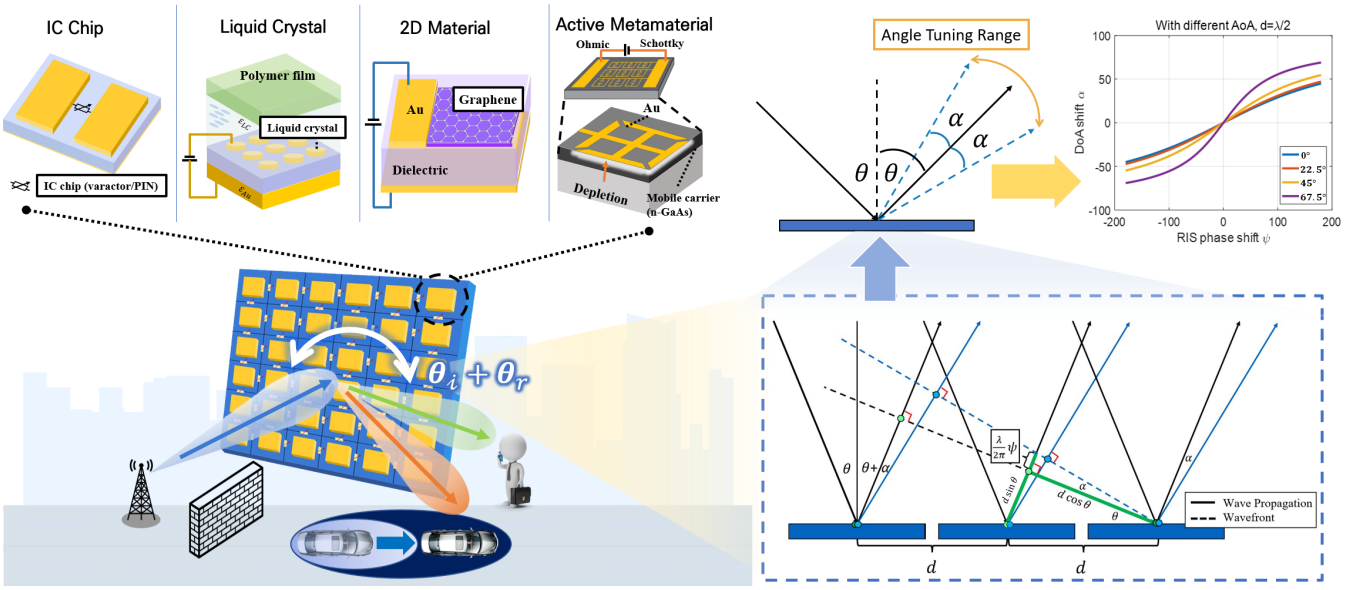

Figure 1. RIS-embedded smart radio network with meta-devices and additional angle tuning range adding to reflection angle via RIS phase shift capability

expanding the scope of SLS in RIS systems, literature that deeply analyzes the design of RIS incorporating meta-devices and tuning capabilities at a system-level is still lacking.

Consequently, this work conducts a comprehensive evaluation of RIS performance via SLS using 3D ray tracing that reflects realistic RIS tuning control ranges. We propose the algorithm capable of performing ray tracing while accounting for the reflection characteristics of RIS, and analyze the system gains in indoor and outdoor scenarios. In particular, we compare and analyze the implications of RIS deployment on milli-meter wave (mmWave) and sub-terahertz (sub-THz), the target frequencies of 6G. As a result, we convincingly demonstrate the performance of various RIS designs, reflecting the tuning capabilities of different meta-devices, at the system-level for the first time.

We summarize the main contributions of this study and explain their interrelationships as follows:

This article addresses the research gap of bridging device-level RIS design with large-scale performance evaluation. Considering the limitations of existing RIS designs, we present various candidate meta-devices with different tuning methods, notably introducing the rarely mentioned electrowetting-based approach. We compile the physical capabilities and characteristics of each device, calculating the relationship between phase shift range and reflection angle shift through geometric modeling. Subsequently, we propose a ray tracing methodology for SLS integrated with RIS and quantitatively analyze the impact of differences in beam tuning capabilities on communication performance. Furthermore, through this, we present guidelines for the implementation and application of potential RIS designs for desired performance in various communication scenarios and standardization standpoint.

II. RIS-EMBEDDED RADIO SYSTEM ANALYSIS

A. RIS Wave Reflection Control and Beam Tuning Model

The properties and modifications of the wave incident on the RIS are determined by the boundary condition at the interface of the surface. Therefore, application of boundary condition can derive the relationship between the reflection coefficient and either refractive index or load impedance.

When the wave impinges on the RIS array, it interacts with the tunable device with specific properties, resulting in scattering of different waves. Therefore, a new component is added to the effective refractive index and impedance, and a corresponding abrupt phase shift ψ is generated. Then RIS with $M \times N$ unit cell array exhibits a phase tuning matrix $\mathbf{\Psi}$, and each additional phase shift affects the new boundary condition. This makes it possible for the reflection angle of the impinging wave to be different from the incidence angle, leading to a generalized laws of reflection considering the phase discontinuity of interfaces. In this article, we assume far-field signal modeling.

Then, the effect of additional phase shift of RIS on the reflection angle can be considered through geometric modeling. As shown in Fig. 1, for a ray impinging at an angle θ_i on an RIS with unit cell inter-distance d, the phase shift of the ray is given by $d \sin \theta_i$ multiplied by the wavenumber $2\pi/\lambda$. Upon reflection, a phase shift ψ induced by the RIS is added to the ray. Geometrically, this corresponds to a physical distance addition as determined by the relationship between electrical length and physical length, which involves multiplying by the reciprocal of the wavenumber, $\lambda/2\pi$. This propagation shift $\psi \cdot \lambda/2\pi$ includes an additional angle tuning α, and this value geometrically holds a tangent relationship with the angle α. Thus, the reflected ray propagates at an angle $\theta_r = \theta_i + \alpha$, where α can be expressed as $\alpha = \tan^{-1}(\lambda\psi/2\pi d \cos\theta_i)$.

That is, the additional angle tuning α, is determined by the phase shift of RIS and can be calculated complementary to each other as expressed above. Since α is influenced by the incident angle, unit cell inter-distance, and the phase shift range of the RIS, generally, the tunable angle range increases when either θ_i or $|\psi|$ is large as visible in the top right of Fig. 1. Specifically, in a scenario where $\theta_i = 45^\circ$ and $d = \lambda/2$, if the RIS can cover a phase shift range from $-\pi$ to

Table I
COMPARISON OF DIFFERENT BEAM TUNING META-DEVICES

	Operation frequency	Modulation speed	Phase tuning range	Mechanism	Energy efficiency	Cost efficiency	Ref
Varactor	GHz	up to GHz	70%	Electrical	High	Medium	[5]
PIN diode	GHz to THz	5 MHz	50%	Electrical	Medium		[3]
2D materials	THz to visible	100 kHz	47%	Electrical	High	Low	[4]
		20 GHz	95%	Electrical			[11]
		40 MHz	60%	Electrical			[4]
Liquid crystals	GHz to visible	20 Hz	15%	Electrical	High	High	[4]
		N/A	18%	Optical			[4]
		N/A	69%	Electrical			[9]
Active metamaterial devices	THz to visible	377 Hz	60%	Electrical	Low	Medium	[12]
		N/A	79%	Electrical			[4]
Electrowetting	GHz to visible	76 Hz	up to 90%	Electrical	High	High	[13]

π, then α can span a range denoted as $\alpha \in [-54.7\,^\circ, 54.7\,^\circ]$. Consequently, the reflection angle θ_r would then fall within the range of $\theta_r \in [-9.7\,^\circ, 99.7\,^\circ]$. Here, the phase shift of RIS covering from 360° full range is required, the value at this time becomes the upper bound of wavefront angle control through RIS. The main lobe angle of the reflected beam, which is shaped by the superposition of the wave through the phase control of each unit cell, also exists within this range.

However, in practice, there is no device technology that can make a phase shift of 100%, so the range of propagation angle that can be controlled is limited. If the phase shift range of the device is 50%, α is significantly reduced to $\alpha \in [-35.2\,^\circ, 35.2\,^\circ]$. This angle control limit results in performance degradation in sweeping or beam tracking for beam selection, and also affects coverage and spectral efficiency obtained by RIS. Therefore, in the remaining parts, this article explores the phase and angle tuning characteristics according to the properties of the meta-devices used to design the RIS and analyzes the relationship with the communication performance.

B. Diode-Driven Tuning Device: Limitation and Challenges

The scheme applied to most RIS designs is a method of controlling the load impedance of the device while adjusting the capacitance and resistance components in the circuit through an external voltage. Several RIS designs use diodes, specifically varactor or Positive-intrinsic-negative (PIN) diode devices. Such devices are currently adopted in most RIS designs due to their fast response speed and ease of control. However, the existing diode-driven RIS design has several limitations and challenges that affect its commercialization in actual B5G/6G networks.

First, a varactor diode is a variable capacitance device that responds to an applied bias and is driven through a reverse voltage. At this time, since the capacitance decreases in inverse proportion to the square root of the reverse voltage, a higher voltage is needed to obtain the same capacitance difference at the margin of the bias range. Consequently, when the applied voltage increases beyond a certain level, the capacitance of the varactor diode-based device approaches a constant value. This leads to the phase tuning of the varactor diode exhibiting a saturation region, which is lower than 2π. According to the measurement results, the phase shift is saturated at above $15\,V$, and has a tuning range limit of below 70% [5].

A PIN diode is, as the name suggests, a device composed of a P-type junction, intrinsic region, and N-type semiconductors. Thus, the PIN diode operates as a switch-like tuning mechanism with a phase shift of 0 and π. Due to this discrete phase shift structure, it is impossible to obtain the specific value required for each RIS element and achieve accurate beam tuning, resulting in performance degradation. In both the theoretical and simulation results, the discrete tuning design shows a significant drop in its SNR compared to the continuous phase control [3]. Performance degradation can be reduced by designing a device with 2 bits or more by utilizing several PIN diodes in one element. However, the use of a multi-bit device sharply increases the required power consumption, which further increases when more RIS elements are required in high-frequency band. In [6], when the RIS having 256 2-bit elements at 2.3 GHz was fabricated, the power consumption was approximately 153 W. As the power required for operation increases, the advantage of RIS over existing phased array or relay decreases, indicating the importance of achieving energy efficiency.

Furthermore, achieving such diode-based devices becomes more challenging as the operating frequency increases. In terms of packaging and manufacturing, diode-driven RIS is not feasible due to its low yields and high cost. In addition, they are hard to be utilized in high-frequency band communications due to the limited cutoff frequency and dramatically increasing loss. In summary, there are limitations in applying conventional diode-based RIS devices to core bands of 6G communication, such as mmWave and sub-THz. Therefore, several feasible methodologies are required to compensate for the limitations of existing designs in the perspective of commercialization and RIS management.

III. RIS WITH POTENTIAL TUNABLE META-DEVICES

A. RIS Design and Analysis with Candidate Meta-devices

Fig. 1 presents the meta-devices to be integrated into the design of the RIS unit cell in this study. Among various reconfigurable devices, methods capable of electrical tuning and applicable in the mmWave or sub-THz bands have been selected. Then we explored each proposed design according to

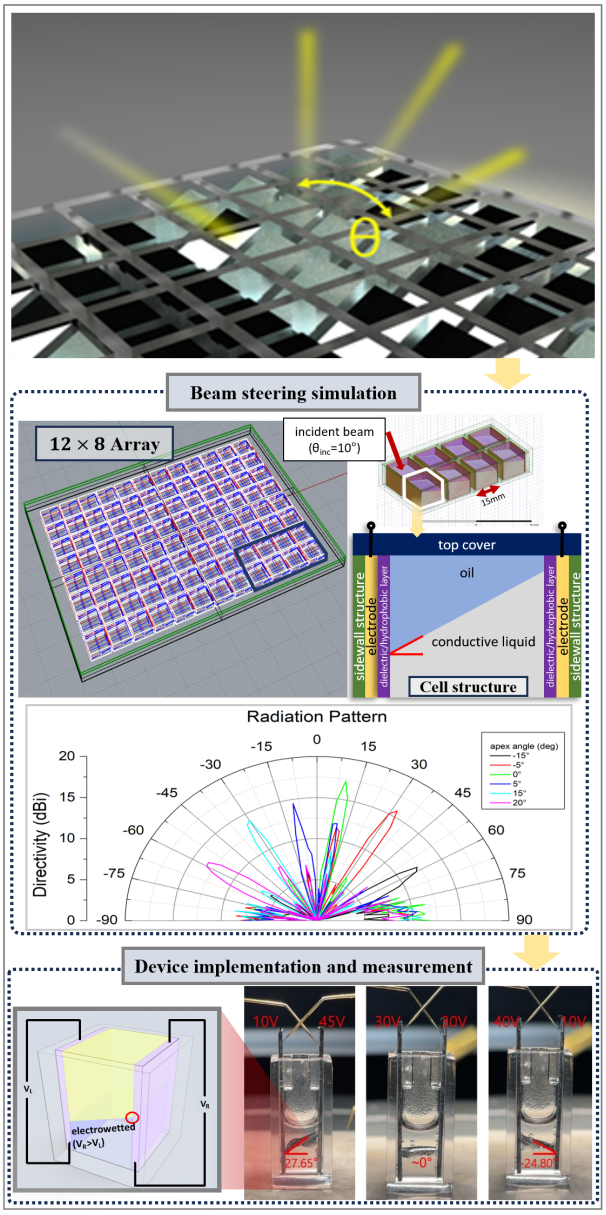

Figure 2. Implementation of electrowetting-based RIS device design and beam tuning operation.

the operation frequency, modulation speed, and tuning range values, energy&cost efficiency and presented the results in Table I. For this table, [4] and multiple other papers on device implementation including [9]–[13] have also been consulted. While this is not an exhaustive survey, it provides a valuable comparison by analyzing candidate devices with different properties and parameters from a communication perspective.

Firstly, among the meta-devices excluding those based on diodes, liquid crystal (LC)-driven devices are the most prominently researched. With a change in the electric field through the external bias, the LC phase dynamically changes, and is accompanied with a change in the effective refractive index, thus enabling the steering of wave. Compared to diodes, LC-based devices can be used scalably in any operating frequency band. In addition, it has a continuous variable range to obtain the desired reflection coefficient. LC is economically beneficial via enabling mass production and can also achieve beam steering with lower power consumption. The disadvantage of LC is the slow response time, ranging from less than 1 Hz to about 20 Hz, making the beam modulation speed insufficient for use in dynamic communication scenarios. In our team's prior work, LC-based RIS implementation and demonstration was conducted within both mmWave and sub-THz [9], [10].

It is possible to manipulate wave interaction through 2D materials with high electrical efficiency, and many meta-device studies using graphene, which obtains high carrier mobility through a band gap close to zero, are being conducted. 2D materials can easily tune the Fermi level with a small gate voltage, resulting in higher energy efficiency than diode-based devices. In [11], the device is composed of optical antenna and graphene to tune the wave by the critical coupling condition change according to the applied gate voltage and obtain a tuning range of about 95%. As such, beam tuning devices using 2D materials have high power efficiency and high tuning capacity. However, there are limitations that it is difficult to apply to the current communication frequency due to the high frequency band mainly being studied, and the fabrication cost is also high.

In addition, meta-device utilizing active THz materials are predicated on semiconductor materials capable of modulating carrier charge densities. This design involves positioning a gold resonator on an n-type gallium arsenide (GaAs) layer, with its operational principle centered around controlling the depletion of carriers within the gap region [12]. Consequently, it can vary conductivity and permittivity to tune the beam through the applied bias without requiring transistors. While active THz materials can attain a high tuning range, they necessitate high voltage and power consumption, and incur elevated implementation costs. Additionally, the modulation speed varies considerably depending on the design.

B. Electrowetting-Based Design

In this article, we proposed a new electrowetting-based-device for beam tuning. To the best of our knowledge, there have been very few reports to introduce electrowetting devices for RIS, and this study is the first to apply a liquid metal-based prism-structure design in mmWave. As depicted in Fig. 2, electrowetting controls the movement of a reflective surface placed between two immiscible liquids.

The proposed electrowetting prism device incorporates a reflective surface that can be actively tilted by applying a bias. Through full-wave electromagnetic simulations using Ansys HFSS, we observed various beam steering angles, with the reflected angle ranging from -58° to 58° when subjected to a 28 GHz wave with an incident angle of 10°. The simulations were conducted in a 12×8 array with each cell sized at 7 mm×7 mm×3 mm. To validate the beam tuning capability, we implemented a unit cell based on electrowetting devices. Fig 2 illustrates the geometric structure and maximum tunable angle. The conductive liquid, oil, and dielectric layer were fabricated using eutectic GaIn with a bulk conductivity of 3.4×10^6, dodecane with a refractive index of 1.41, and SiO_2 with a refractive index of 2.1, respectively. From our measurements, a maximum reflective surface tilt of -24.8° to 27.65°

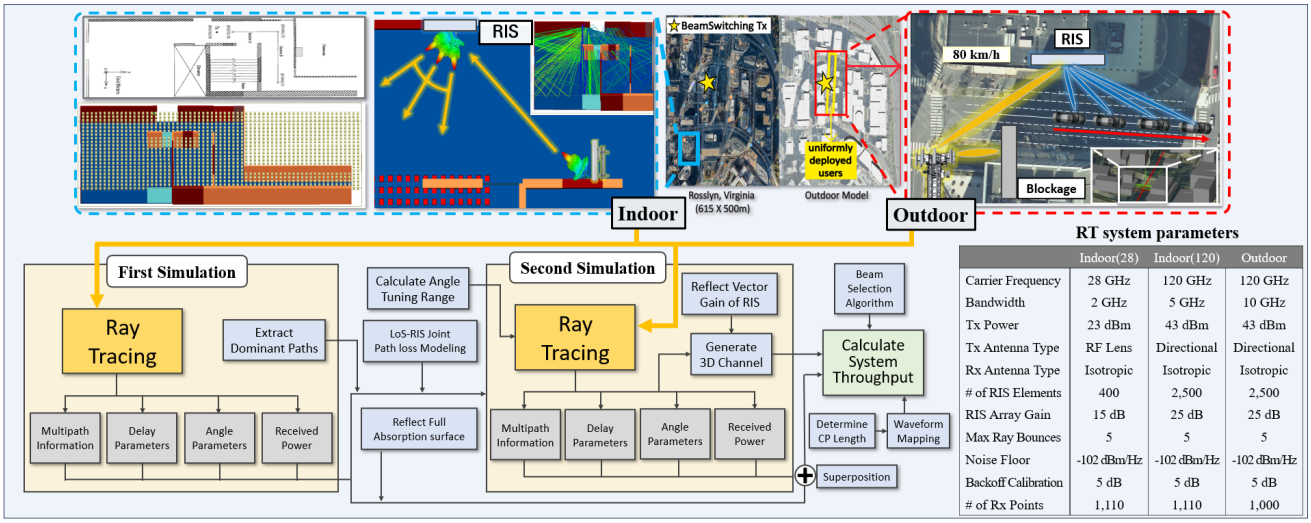

	Indoor(28)	Indoor(120)	Outdoor
Carrier Frequency	28 GHz	120 GHz	120 GHz
Bandwidth	2 GHz	5 GHz	10 GHz
Tx Power	23 dBm	43 dBm	43 dBm
Tx Antenna Type	RF Lens	Directional	Directional
Rx Antenna Type	Isotropic	Isotropic	Isotropic
# of RIS Elements	400	2,500	2,500
RIS Array Gain	15 dB	25 dB	25 dB
Max Ray Bounces	5	5	5
Noise Floor	-102 dBm/Hz	-102 dBm/Hz	-102 dBm/Hz
Backoff Calibration	5 dB	5 dB	5 dB
# of Rx Points	1,110	1,110	1,000

Figure 3. An illustration of the proposed RIS integrated ray tracing simulation topologies, algorithm, and system parameters.

was obtained. Although the operation of the electrowetting method achieves tuning by altering the angle of the reflective surface rather than directly changing the wave's phase, it can be effectively converted using the geometric modeling relationships in II-A. Based on an incidence angle of 45°, converting the maximum surface tilt value from the above experiment into its impact on the reflection angle through the formula shows results equivalent to tuning the phase between [-184°, 150°]. This corresponds to approximately 93% of the phase tuning range.

Electrowetting devices can be compared to LC in terms of materials and processes, with both being energy-efficient and capable of achieving high cost-efficiency through mass production processes in the display industry. Unlike LC, which is limited by the refractive indices of the liquid, electrowetting offers a wider beam steering range. Additionally, from an operational perspective, electrowetting is partially similar to micro-electro-mechanical systems (MEMS). Both are energy-efficient, but MEMS entails notably high manufacturing costs. Moreover, compared to most devices where the reflective area of the array is limited by actuation parts, the proposed electrowetting prism device can utilize the majority of the array area as the reflective surface. Response times for electrowetting reported to date are on the scale of tens of milliseconds, with the result exhibited at 13 ms (76 Hz) as detailed in [13]. Furthermore, there is significant potential to further expand the modulation speed through efforts in cell miniaturization, viscosity control, and optimization of hydrophobic coatings.

IV. 3D System-Level Evaluation

The meta-devices previously discussed possess a range of parameters and associated tuning capabilities, as detailed in Table I. In this section, we investigate the relationship between these physical attributes and communication performance at a system-level through a large-scale approach employing 3D ray tracing. Thus, we aim to bridge the gap between device requirements and system gains essential for RIS design.

A. Ray-Tracing in RIS-based Intelligent Reflective Radio

A previous study reported the difficulties in performing RIS analysis through ray tracing due to the modeling of existing wave transformation based on conventional laws of reflection in built-in software [1]. In other words, most current ray tracing tools cannot apply generalized laws of reflection, preventing the simulation of unnatural propagation with different angles of incidence and reflection. To address this, we propose an alternative methodology that utilizes the geometric model of ray tracing by applying a kind of divide-and-conquer approach. This algorithm treats the RIS as both a receiving and a transmitting source in a sequential simulation, resulting in a combined outcome. Here, the first simulation's output is used as the setup input for the second simulation, capitalizing on the ray tracing characteristic that can derive radio parameters for each ray from transceivers.

In the first simulation, the base station is set as a point type transmitter, and the RIS becomes a point type receiver at the deployed location, with the transmitter's main beam aligned toward the RIS. Thereafter, Ray tracing is executed over the designed terrain, focusing on extracting only the LoS and first-order paths, while all other reflected rays are discarded. This process is reflective of the severe signal attenuation characteristics of the target frequency band, ensuring only paths close to LoS affect the RIS. Furthermore, since rays incident on the physical surface area of the RIS will not undergo specular reflection, a surface made of full absorption material of the same size as the actual area, centered around the point location of the RIS, is installed to eliminate the propagation effects within the designated parts. Afterwards, delay spread, path loss, received power, angle-of-departure (AoD), and angle-of-arrival (AoA) parameters are obtained from the output data for use in subsequent simulations and throughput calculations.

In the subsequent trial, the main simulation is conducted for the performance evaluation. The RIS's transmitter point is now placed at the receiver location from the first simulation. Considering downlink multi-user beamforming with RIS-reflected links, the receivers are deployed in a grid pattern throughout the digital map to assess large-scale system cover-

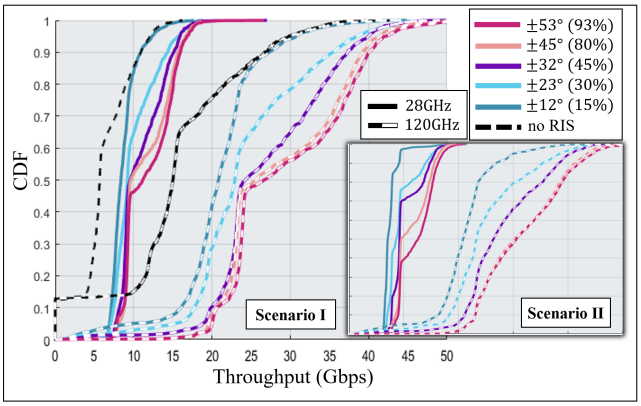

Figure 4. 3D performance evaluation results obtained through the proposed methods. It showcases the CDF for the indoor scenario, considering different phase tuning ranges. The results are presented for a fixed beam number and fixed beamwidth at both 28 GHz and 120 GHz frequencies.

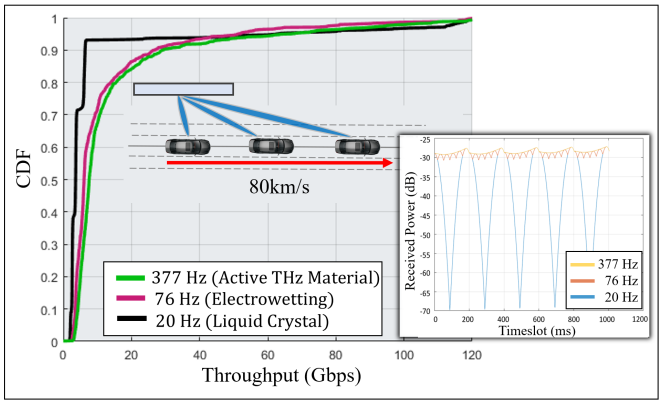

Figure 5. CDF results of the outdoor scenario for mobile beam tracking with different device beam modulation speed and received power at each time slot of the outdoor scenario for each RIS devices.

age and overall throughput. At this stage, the RIS is capable of adjusting the wave reflection angles as required, with the angle tuning range calculated by the AoA and phase tuning range of the RIS device according to the relationship outlined in Sec.II. Furthermore, since the first-order reflected power is close to LoS when RIS is present, the path loss and received power obtained in the previous step are modeled through the approach in [14] rather than by the summation of individual path losses. Here, we incorporate the array gain that reflects the vector summation according to the number of elements in the RIS as a post-processing step. Finally, the performance is compared and analyzed through the superposition of paths with and without the RIS.

Fig. 3 illustrates the 3D system-level simulation algorithm of the proposed RIS-embedded network. To simulate the communication performance of various RIS designs, we apply the manipulation variables of each meta-device in Table I to the RIS beam selection and beam tracking algorithm. Subsequently, a 3D channel parameter set and a beam steering vector are formulated for each operating frequency. Following this, the throughput performance, utilizing the dominant beam selection algorithm, is analyzed.

B. 3D Performance Evaluation of Indoor/Outdoor Simulations

In our simulations, we utilize Remcom's Wireless Insite software to conduct performance analysis in a realistic environment. To provide a comprehensive comparison from different perspectives, we consider the following scenarios:

1) Indoor beam selection with the same number of beams
2) Indoor beam selection with identical beam intervals.
3) Outdoor beam tracking with mobility-aware vehicles.

To model scenarios 1 and 2, we introduce an indoor environment that considers realistic geometry and materials. The indoor surrounding is modeled as 9.5 m×27 m×3.3 m indoor space as displayed in Fig. 3, taking into account the frequency-sensitive properties of materials. Our ray tracing simulations are performed for different center frequencies, specifically 28 GHz and 120 GHz. The location of the transmitter is set at (2.9, 9.9, 2) from the reference (0, 0, 0), and the location of the RIS is (0.2, 7.2, 2). There are a total of 1,110 receiver points with 0.25 m spacing and detailed radio parameters are illustrated in Fig. 3.

First, we apply the same number of beams in each simulation to analyze system performance via beam sweeping through the RIS. The RIS propagated signal is reflected from the transmitter, and a total of eight beams are formed. When there is no RIS, the transmitter immediately sweeps through the same number of beams. This setup aims to evaluate the impact of the RIS's tuning capabilities on communication performance, distributing the beams evenly according to the angle tuning ranges of various meta-devices. The incident angle is based on 45 °, and the phase tuning range of [15% 30% 45% 80% 95%] is converted into angle tuning range of [12 ° 23 ° 32 ° 45 ° 53 °], respectively. At this point, the 93% phase tuning range corresponds to the experimental maximum tuning value of the electrowetting prism device implemented in this study, as described in III-B. In other words, when the angle tuning of the devices differs, the range at which the main beam direction can point changes, and accordingly, the received power by users distributed on the grid varies.

In the second scenario, the simulation is performed by standardizing the inter-beam interval to reflect the half power beamwidth (HPBW) of the selected beam pattern. Further details on the beam interval and HPBW used in this simulation is detailed in the document [15]. The settings for the incident angle and the phase/angle tuning range are the same as in scenario 1. Dividing each angle tuning range by the utilized beam spacing, [2 4 5 7 9] beams were used in 28 GHz, and [8 14 19 27 32] beams were used in 120 GHz, respectively.

For the third scenario, a 1 km×1 km 3D digital map of Rosslyn, Virginia, USA, was applied to simulate an urban environment as shown in Fig. 3. What we want to analyze in the outdoor scenario is evaluating how effectively the RIS can track a moving Rx when mobility is considered. In Scenario 3, only the sub-THz band is utilized, accounting for narrow beams. The RIS location is set at (630, 745, 8.5) on the wall of a building, and the initial distance to the Rx point is approximately 15 m. The receivers are modeled as a moving trajectory, resembling a vehicle traveling at a constant speed of 80 km/h along the predefined road. Snapshots are taken every 1 ms, tracking all receiver points for each time slot, resulting in a total of 1,000 points being calculated. The beam

tracking must adjust to a different angle in each timeslot, so the beam modulation speed of the RIS must be sufficiently rapid, otherwise, precise beam tracking cannot be achieved. For this purpose, the modulation speed of actual RIS candidate meta-devices is a critical factor. The selected modulation speeds are 20 Hz, 67 Hz, and 377 Hz for liquid crystal, electrowetting, and active metamaterial, respectively, excluding devices with sufficiently high speed. In the outdoor scenario, ray tracing is conducted using the proposed algorithm, and the overall system throughput is assessed by accumulating and analyzing the points from each timeslot.

C. Performance Results Analysis

Initially, the impact of the phase tuning range (angle tuning range) of the meta-device on communication performance was assessed using scenarios 1 and 2, as shown in Fig. 4. In all simulations, a broader angle scanning range by the RIS correlated with higher throughput performance, with more pronounced results as the tuning capability difference increased. In mmWave, the result of $\pm$ 53 $^\circ$ device (electrowetting) achieved a performance gain of approximately 5 Gbps in over 50% of the area compared to $\pm$ 12 $^\circ$ device. In addition, direct beamforming from the transmitter, in the absence of RIS, resulted in reduced performance due to the characteristics of the indoor environment with high carrier frequency and blockage. In the sub-THz band, a remarkable performance gain of up to 15 Gbps was observed in devices with a higher tuning range compared to those with lower tuning capabilities. In an additional scenario with unified beamwidth, changes in the overall system throughput were noted because the number of beams used for each simulation was different. The performance difference based on device properties became more significant, and the system gain was notable even in areas below 50% of the CDF.

The study confirmed the relationship between the phase tuning capability and the overall throughput gain, and quantitatively analyzed this relationship on communication performance. Notably, this effect was more significant when using sub-THz as the carrier frequency. Standardizing the beam spacing considering the HPBW resulted in more pronounced distinctions in device performance across all receivers. These findings facilitate a reliable analysis of the coverage enhancement achievable through the tuning capacity of RIS from a system-level performance perspective.

Through Scenario 3, the beam tracking performance of RIS in a mobility-reflective environment was assessed. This simulation investigated the impact of RIS's beam modulation speed on real-time tracking performance. As demonstrated in Fig. 5, compared to the previous scenarios, there was no substantial difference in the performance of mobile user beamforming with changes in device characteristics. It is understood that, given the realistic outdoor Tx-Rx distance and angle, even if the receiver moves rapidly, the difference in the actual distance changed within a timeslot of few milliseconds is minimal. This means that even if slightly off the main direction, there exists a time range that the sub-THz beamwidth can adequately cover, and as the beam response time becomes faster, more receivers will be present within this area. To intuitively understand this, each simulation in Fig. 5 illustrates the attenuation of received power depending on the receiver's position (timeslot). It was also observed that beam modulation speeds over 76 Hz, corresponding to the electrowetting device, achieved adequate beam tracking without notable degradation compared to the faster kHz-scale response speeds.

V. Guidelines for RIS Standardization and Implementation

RIS has not yet been included as a study item in 3GPP Release 18 and earlier 5G standardization processes, an ETSI Industry Specification Group (ISG) for RIS was established, providing technical tasks for pre-standardization [2]. According to their first group report (ETSI GR RIS-001), RIS is identified as a key requirement by various stakeholders for its energy conservation and cost efficiency, distinguishing it from existing infrastructure. Additionally, synthesizing the shared perspectives of GR RIS-002 and 003, it is possible to conclude the necessity for extensive PoC, which includes the creation of extended and accurate models reflecting the realistic nature and integration with existing technology frameworks. These standardization efforts aim to ensure the interoperability and seamless deployment of RIS in future wireless networks. This article aims to ensure that RIS technology aligns with accepted standards and encourages the exploration of new research directions to further refine RIS capabilities.

Energy Efficiency PoC Analysis: To accelerate the standardization discussions on RIS, it is crucial to conduct extensive empirical studies on energy efficiency in addition to communication aspects such as throughput. Implementing various meta-devices and dedicated control boards in diverse deployment scenarios to collect substantial quantitative data on actual power performance in natural-like systems is essential.

Productivity and Economic Efficiency: In high-frequency bands, RIS arrays are composed of hundreds to hundreds of thousands of unit cells, necessitating efforts to ensure sufficient production capacity and economic feasibility of the component devices. For electrowetting devices, leveraging process development in conjunction with the display industry, where electrowetting has been used, can provide the competitive edge needed for establishing mass production lines and achieving cost efficiency.

Design for Practical Deployment: Numerous commercial scenarios anticipate that RIS will be attached to existing infrastructure such as walls and windows. It would be beneficial to develop meta-devices for RIS with transparent, flexible, and easy-to-maintain to enable realistic and aesthetically pleasing deployments.

VI. Conclusion

This article proposed practical and effective approaches for developing RIS systems from a device-to-communication perspective. Our modeling calculates the upper bound of the RIS's angle of reflection using device tuning capacity, surpassing ideal phase modeling and enhancing practicality. We introduced potential RIS designs based on meta-devices to overcome limitations of diode-based devices, and explored

new possibilities in energy, cost, and feasibility. Our innovative electrowetting-based RIS design expands implementation possibilities. Through system-level simulations on 3D urban scenarios, we demonstrated performance gains of RIS-embedded systems. Our SLS methodology and evaluation provided intuitive RIS design insights for new devices and network scenarios. We believe that these efforts will position RIS as a feasible phase to the standardization for B5G/6G.

ACKNOWLEDGEMENTS

The work was in part supported by IITP grant funded by the Korea government (MSIT) (No. 2021-0-00486, 2021-0-02208, 2024-00428780) and by the National Science Foundation under Grant No. NSF-ECCS-2435261and the Army Research Office under Grant W911NF2410107.

References

[1] M. Di Renzo *et al.*, "Smart radio environments empowered by reconfigurable intelligent surfaces: How it works, state of research, and the road ahead," *IEEE J. Sel. Areas Commun.*, vol. 38, no. 11, pp. 2450-2525, Nov. 2020.

[2] C. K. Wen *et al.*, "Shaping a smarter electromagnetic landscape: IAB, NCR, and RIS in 5G standard and future 6G," *IEEE Commun. Stand. Mag.*, vol. 8, no. 1, pp. 72-78, Mar. 2024.

[3] Q. Wu, R. Zhang "Beamforming optimization for wireless network aided by intelligent reflecting surface with discrete phase shifts," *IEEE Trans. Commun.*, vol. 68, no. 3, pp. 1838–1851, Mar. 2020.

[4] A. Nemati, Q. Wang, M. Hong, and J. Teng "Tunable and reconfigurable metasurfaces and metadevices," *Opto-electron. Adv.*, vol. 1, no. 5, 180009, Jun. 2018.

[5] X. Pei *et al.*, "RIS-aided wireless communications: Prototyping, adaptive beamforming, and indoor/outdoor field trials," *IEEE Trans. Commun.*, vol. 69, no. 12, pp. 8627-8640, Dec. 2021.

[6] L. Dai *et al.*, "Reconfigurable intelligent surface-based wireless communications: Antenna design, prototyping, and experimental results," *IEEE Access.*, vol. 8, pp. 45913–45923, 2020.

[7] J. Huang, C. X. Wang, Y. Sun, J. Huang, and F. C. Zheng, "A novel ray tracing based 6G RIS wireless channel model and RIS deployment studies in indoor scenarios," in *Proc. IEEE Int. Symp. Pers. Indoor Mobile Radio Commun. (PIMRC).*, pp. 884–889, Sep. 2022.

[8] B. Sihlbom, M. I. Poulakis, and M. D. Renzo, "Reconfigurable intelligent surfaces: Performance assessment through a system-level simulator," *IEEE Wireless Commun.*, vol. 30, no. 4, pp. 98–106, Aug. 2023.

[9] Y. Youn *et al.* "Liquid crystal-driven reconfigurable intelligent surface with cognitive sensors for self-sustainable operation," *IEEE Trans. Antennas Propag.*, vol. 71, no. 12, pp. 9415–9423, Dec. 2023.

[10] D. Jun *et al.* "Real-time implementation of semi-active reconfigurable intelligent surfaces for mmWave and sub-THz systems," in *Proc. IEEE Consumer Commun. and Net. Conf. (CCNC).*, pp. 941-942, Feb. 2023.

[11] Y. Yao *et al.*, "Electrically tunable metasurface perfect absorbers for ultrathin mid-infrared optical modulators," *Nano Lett.*, vol. 14, no. 11, pp. 6526–6532, Oct. 2014.

[12] H. T. Chen *et al.*, "A metamaterial solid-state terahertz phase modulator," *Nat. Photonics.*, vol. 3, no. 3, pp. 148–151, Feb. 2009.

[13] R. A. Hayes, and B. J. Feenstra, "Video-speed electronic paper based on electrowetting," *Nature.*, vol. 425, pp. 383–385, Sep. 2003.

[14] E. Basar *et al.*, "Wireless communications through reconfigurable intelligent surfaces," *IEEE Access.*, vol. 7, pp. 116753-116773, 2019

[15] M. Giordani, M. Polese, A. Roy, D. Castor, and M. Zorzi, "A tutorial on beam management for 3GPP NR at mmWave frequencies," *IEEE Commun. Surveys Tuts.*, vol. 21, no. 1, pp. 173–196, 1st Quart., 2019.